19

The Viscosity of Carbonate-Silicate Transitional Melts at Earth's Upper Mantle Pressures and Temperatures, Determined by the In Situ Falling-Sphere Technique

Vincenzo Stagno[1,5], Yoshio Kono[2,3], Veronica Stopponi[1], Matteo Masotta[4], Piergiorgio Scarlato[5], and Craig E. Manning[6]

ABSTRACT

The circulation of carbon in Earth's interior occurs through the formation, migration, and ascent of CO_2-bearing magmas throughout the convective mantle. Their chemical composition spans from carbonatitic to kimberlitic as a result of either temperature and pressure variations or local redox conditions at which partial melting of carbonated mantle mineral assemblages occurs. Previous experiments that focused on melting relations of synthetic CO_2-bearing mantle assemblages revealed the stability of carbonate-silicate melts, or transitional melts, that have been generally described to mark the chemical evolution from kimberlitic to carbonatitic melts at mantle conditions. The migration of these melts upward will depend on their rheology as a function of pressure and temperature. In this study, we determined the viscosity of carbonate-silicate liquids (~18 wt% SiO_2 and 22.54 wt% CO_2) using the falling-sphere technique combined with in situ synchrotron X-ray radiography. We performed six successful experiments at pressures between 2.4 and 5.3 GPa and temperature between 1565 °C and 2155 °C. At these conditions, the viscosity of transitional melts is between 0.02 and 0.08 Pa˙s; that is, about one order of magnitude higher than what was determined for synthetic carbonatitic melts at similar P-T conditions, likely due to the polymerizing effect of the SiO_2 component in the melt.

19.1. INTRODUCTION

The cycling of carbon in the Earth's interior occurs in part through the ascent of carbonated magmas, in which the presence of variable amounts of CO_2 depends on the degree of partial melting, as controlled by pressure, temperature, and mantle oxidation state (Brey et al., 2008; Brey et al., 2011; Dalton & Presnall, 1998; Dasgupta et al., 2013; Gudfinnsson & Presnall, 2005; Hammouda & Keshav, 2015; Kiseeva et al., 2012, 2013; Litasov & Ohtani, 2009a, 2009b; Litasov & Ohtani, 2010; Stagno & Frost, 2010; Stagno et al., 2013). Experimental studies showed that carbonatitic melts produced by low degrees of partial melting of carbonated mantle rocks evolve to carbonate-silicate melts as the degree of partial melting increases from less than 0.1% to about 1% (Dasgupta et al., 2013). In the present-day convective mantle, carbonate-silicate melts with SiO_2 content between 10 and 25 wt% are likely to form by extensive redox melting of a graphite-bearing peridotite at 75–100 km depth within –1.8 log units < fo_2 (normalized to FMQ buffer) < –2.5 log units (Stagno et al. 2013), while they likely formed at

[1] *Dipartimento di Scienze della Terra, Sapienza Universita' di Roma, Italy*
[2] *Geophysical Laboratory, Carnegie Institution of Washington, Argonne, Illinois, USA*
[3] *Geodynamics Research Center, Ehime University, Ehime, Japan*
[4] *Dipartimento di Scienze della Terra, Università di Pisa, Pisa, Italy*
[5] *Istituto Nazionale di Geofisica e Vulcanologia, Roma, Italy*
[6] *Department of Earth, Planetary and Space Sciences, University of California–Los Angeles, Los Angeles, California, USA*

Carbon in Earth's Interior, Geophysical Monograph 249, First Edition. Edited by Craig E. Manning, Jung-Fu Lin, and Wendy L. Mao.

shallower depths and more reduced fo_2 conditions (between FMQ-2.3 and FMQ-3.5 log units) beneath mid-ocean ridges in the Archaean (Aulbach & Stagno 2016), with important implications for the mobilization of oxidized carbon from the interior of Earth to the atmosphere. There is evidence of the stability of carbonate-silicate melts coexisting with mantle minerals from experimental studies performed within simplified carbonated systems like CaO-MgO-SiO_2-CO_2 (Moore & Wood 1998), CaO-MgO-Al_2O_3-SiO_2-CO_2 (Dalton & Presnall, 1998; Gudfinnsson & Presnall, 2005; Keshav & Gudfinnsson, 2014), CaO-MgO-Al_2O_3-SiO_2-Na_2O-CO_2 (Litasov & Ohtani, 2009b; Litasov & Ohtani, 2010), CaO-MgO-Al_2O_3-SiO_2-Na_2O-K_2O-Cl-CO_2 (Litasov & Ohtani, 2009a), CaO-Al_2O_3-SiO_2(±Na_2O)-CO_2 (Brooker & Kjarsgaard, 2011), and more complex systems representative of peridotite (Brey et al., 2008; Brey et al., 2011; Dasgupta & Hirschmann, 2007; Foley et al., 2009; Ghosh et al., 2014; Rohrbach & Schmidt, 2011; Stagno & Frost, 2010) and eclogite (Kiseeva et al., 2012; Kiseeva et al., 2013) mantle assemblages, respectively. These melts span compositions from ~14 to ~30 wt% SiO_2, CO_2 between 15 and 40 wt%, and Ca# (CaO/(CaO+MgO) mole ratio) of 0.5 on average but with a strong variation (±0.3) due to dependence on the coexisting mineral phases and bulk composition of the starting material, especially the alkali content. Transitional melts fall within the field of carbonate-silicate liquids and are characterized by SiO_2+Al_2O_3 varying between ~18 and ~32 wt% (Moussallam et al., 2015). A much narrower chemical variation was proposed by Gudfinnsson and Presnall (2005) with about 15–22 wt% SiO_2, ~0.9–2.6 wt% Al_2O_3, and Ca# of 0.4–0.5. Based on these experimental studies, whose P-T conditions are summarized in Figure 19.1, transitional melts represent a link between near-solidus carbonatitic melts and relatively more SiO_2-rich melilititic and kimberlitic melts (Martin et al., 2013) produced by the melting of CO_2-rich portions of the Earth's mantle at variable depths.

Although P-T conditions required for the stability of transitional melts have been experimentally constrained (Figure 19.1), very little is known about their rheology at depth. The knowledge of the viscosity of carbonate-silicate melts is needed to better constrain their mobility, migration rate (velocity) from the source rock, and the time of melt-rock interaction.

To date, knowledge of viscosity of CO_2-rich melts at high pressure and temperature representative of the mantle is mostly limited to pure carbonate compositions chosen as analogue of natural carbonatitic melts. Dobson

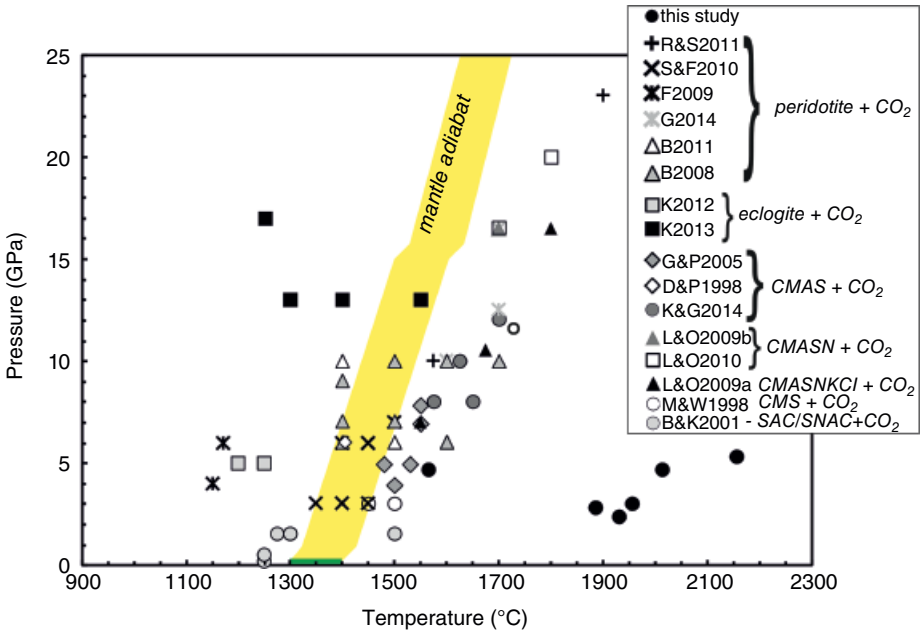

Figure 19.1 Diagram showing temperatures and pressures set for the experiments of this study compared to previous studies where the stability of carbonate-silicate melts with 16–20 wt% SiO_2 was reported, plotted along with the mantle adiabat (Stixrude & Lithgow-Bertelloni, 2007). Black circles are the P-T conditions for the viscosity experiments from this study. Abbreviations for data sources: B2008 = Brey et al., 2008; B2011 = Brey et al., 2011; B&K2001 = Brooker & Kjarsgaard, 2001; D&P2008 = Dalton & Presnall, 1998; F2009 = Foley et al., 2009; G2014 = Ghosh et al., 2014; G&P2005 = Gudfinnsson & Presnall, 2005; K2012 = Kiseeva et al., 2012; K2013 = Kiseeva et al., 2013; K&G2014 = Keshav & Gudfinnsson, 2014; L&O2009a = Litasov & Ohtani, 2009a; L&O2009b = Litasov & Ohtani, 2009b; L&O2010 = Litasov & Ohtani, 2010; M&W1998 = Moore & Wood, 1998; R&S2011 = Rohrbach & Schmidt, 2011; S&F2010 = Stagno & Frost, 2010. See electronic version for color representation of the figures in this book.

et al. (1996) published the first study on viscosity and density measurements of Mg-K and Ca-K carbonate mixtures at conditions of the Earth's mantle obtaining data between 0.06 and 0.036 Pa˙s at 2–5.5 GPa and 800 °C–1500 °C. Kono et al. (2014a) performed an in situ investigation of the viscosity of melts with both calcite ($CaCO_3$) and dolomite ($Mg_{0.40}Fe_{0.09}Ca_{0.51}(CO_3)_2$ compositions up to 6.2 GPa. The study employed an ultrafast synchrotron X-ray camera available at beamline 16 BM-B of Advanced Photon Source (Lemont, Illinois, USA) to record the fall of a platinum sphere at up to 1000 frame˙s^{-1}. Measured viscosities of calcite and dolomite melts were surprisingly low, being in the range of 0.006–0.010 Pa˙s and 0.008–0.010 Pa˙s, respectively. Using the same experimental technique, Stagno et al. (2018) determined even lower viscosities in the range of 0.003–0.007 Pa˙s for Na_2CO_3 melt at mantle pressures and temperatures that raises important questions on the effect of alkali elements on the rheology of carbonatitic magmas. These values are about 2–3 orders of magnitude lower than the measured viscosity of basaltic melts (Sakamaki et al., 2013), suggesting a strong effect of increasing SiO_2 content on the viscosity of magmas. In turn, transitional melts are expected to possess intermediate rheological properties in between basalts and carbonatites. Ghosh and coauthors (Ghosh, Bajgain, et al., 2017; Ghosh & Karki, 2017) investigated the rheological properties of carbonated $MgSiO_3$ melts by first-principle calculations at depths of the core-mantle boundary and temperature up to 5000 K. Extrapolation of their results to upper mantle conditions yields viscosities of ~0.025 Pa˙s. However, this study does not link directly to the chemical composition of carbonate-silicate melts as those obtained in high P-T experiments using the large volume press facilities (Figure 19.1).

We investigated the viscosity of a synthetic carbonate-silicate melt with ~18 wt% SiO_2 and ~22 wt% CO_2 by the falling-sphere technique at high pressure and temperature using the Paris-Edinburgh press combined with in situ synchrotron X-ray radiography at the beamline 16 BM-B of the Advanced Photon Source (Illinois, USA). Our results are compared with those of pure carbonate melts and synthetic basalts with implications for the CO_2 circulation throughout the Earth's interior.

19.2. MATERIALS AND METHODS

Two starting materials were employed in this study, CB2 and CARB2, with composition representative of transitional melts (Gudfinnsson & Presnall, 2005), such as 18.28 wt% SiO_2, 20.43 wt% CaO, 27.50 wt% MgO, 6.72 wt% FeO, 1.95 wt% Al_2O_3, 1.37 wt% Na_2O, 1.21 wt% ClO^-, and 22.54 wt% CO_2. CB2 was prepared by grinding under ethanol oxides and carbonates such as SiO_2, FeO, Al_2O_3, $CaCO_3$, $MgCO_3$, and NaCl to make a nominal composition like the above. CARB2 was prepared by melting CB2 at ~0.3 GPa and 1410(±10) °C for 1 h, using a non-end-load piston cylinder (QUICKPress type) available at the Istituto Nazionale di Geofisica e Vulcanologia (INGV) in Rome (Italy). In the synthesis experiment, the CB2 mixture was loaded into a platinum (Pt) capsule of 5 mm length and 5 mm diameter, welded at both ends. The capsule was loaded into a 19–25 mm crushable MgO-borosilicate glass-NaCl assembly (Masotta et al., 2012). Temperature was constantly monitored during the experiment using a factory calibrated C-type thermocouple, with a maximum error of 5 °C. The run was quenched by shutting down the power. The recovered sample was analyzed by field-emission scanning electron microscopy using a JEOL JSM 6500F, also available at INGV both for textural observations and chemical composition. The sample showed a typical quench texture expected for carbonate-silicate melt compositions, alternating glassy portions with elongated crystals of olivine. Such observation appears in contrast with the well-quenched glass reported by Moussallam et al. (2015) for synthetic transitional melts, and it is likely a consequence of the lower quench rate of the QUICKPress compared to that of the internally heated pressure vessels used by Moussallam et al. However, we decided to use both CARB2 and CB2 oxide mixture to test possible effects of the starting material on viscosity measurements.

Viscosity measurements were conducted using the falling-sphere technique with the Paris-Edinburgh large-volume press at beamline 16-BM-B (Kono et al., 2014b; Kono, 2018). The starting material was placed in a cylindrical graphite capsule with a diameter of 1.2 mm and height of 2 mm. The majority of the experiments were performed using CARB2 starting glass, except in the run at 4.7 GPa/1565 °C, where CB2 oxide/carbonate mixture was employed (Table 19.1). A Pt sphere prepared by arc melting with diameter between ~70 and 190 μm (Table 19.1) was placed in the central portion of the capsule. Some runs were performed using the double-layered probing sphere configuration (Terasaki et al., 2001; runs at 4.7 GPa/1565 °C, 2.8 GPa/1885 °C, 3 GPa/1955 °C), where an additional Pt sphere was placed at the top of the capsule surrounded by $CaCO_3$ powder (calcite, Puratronic®, purity of 99.999%) to delay the fall of the probing sphere at a higher temperature than the sphere placed in the center of the sample, which was used to monitor the onset of melting. Details on the cell assembly used in this study are available in Kono et al. (2014b) and are the same than those used by Stagno et al. (2018). The generated pressure at the sample was constantly monitored using the equation of state of MgO (Kono et al., 2010) by collecting diffraction patterns on the MgO sleeve surrounding the capsule. After compression to target pressure, for each experiment the temperature was set

Table 19.1 Experimental conditions and results.

Run	P[b] (GPa)	T[b] (°C)	ø Pt Sphere (mm)	Terminal Velocity (mm/s)	Recording Time (fps)	Viscosity (Pa·s)	logη	Horizontal shift[a] (mm)
CB2_3_2015	4.7	1565	0.117	1.864(±0.048)	100	0.0529(±0.0007)	–1.277	0.021
CARB2_2_2016	2.8	1885	0.191	4.254(±0.165)	500	0.0510(±0.0016)	–1.292	0.075
CARB2_3_2016	4.7	2012	0.140	3.611(±0.088)	500	0.0368(±0.0014)	–1.434	0.030
CARB2_1_2018	3	1955	0.089	2.687(±0.170)	500	0.0228(±0.0018)	–1.642	0.008
CARB2_2_2018	2.4	1930	0.086	0.749(±0.030)	167	0.0762(±0.0030)	–1.118	0.011
CARB2_5_2018	5.3	2155	0.140	6.628(±0.259)	500	0.0202(±0.0008)	–1.695	0.022

[a] Horizontal shift refers to a lateral shift of the Pt sphere during the fall that might result in decrease of the terminal velocity.
[b] Typical uncertainties on pressure and temperature in the Paris-Edinburgh cell experiments are less than 0.4 GPa and 60 °C (e.g., Kono et al., 2014a; de Grouchy et al., 2017; Hudspeth et al., 2018).

quickly (~100 °C/s) to the value at which the platinum sphere fell down and was estimated using the power vs. temperature calibration curve corrected for the proper hydraulic pressure (Kono et al., 2014b).

Viscosity measurements were conducted using the falling-sphere technique combined with unfocused white X-ray beam for radiographic images captured by a high-speed camera (Photron FASTCAM SA3) with 100–500 frames per second (fps) recording time (Kono et al., 2014b; Kono, 2018). The image resolution of the ultra-fast camera used for the viscosity measurements is 2.5 μm/pixel except for the run at 4.7 GPa/1565 °C (CB2_run3_2015), whose resolution is 5 μm/pixel. The radiographic images acquired from the high-speed camera were used to calculate the probing sphere terminal velocity as a function of elapsed time for each frame by using the Tracker plugin in the ImageJ software (Abramoff et al., 2004); and from the velocity of the falling sphere(s), the melt viscosity was calculated using the Stokes equation,

$$\eta = \frac{gd^2\left(\rho_s - \rho_l\right)}{18\upsilon}\frac{F}{E}, \qquad (19.1)$$

where ν is the terminal velocity (mm/s) of the probing sphere; ρ_s and ρ_l are the densities (g/cm^3) of the Pt sphere (~19.3 g·cm^{-3} as calculated from the thermal equation of state; Dorogokupets & Dewaele, 2007) and melt, respectively; d is the diameter of the sphere (mm) determined from the radiographic images using the Prosilica GC1380 high-resolution camera with pixel size of 0.945 μm/pixel (0.850 μm/pixel for runs at 2.4 GPa/1930 °C, 5.3 GPa/2155 °C, 3 GPa/1955 °C); and E and F are correction factors for the wall effect and end effect, respectively. A fixed value of 2.3 g·cm^{-3} was chosen for the density of carbonate-silicate melts (ρ_l), as determined by numerical simulation by Ghosh et al. (2017). This value is slightly greater than the density of 2 g·cm^{-3} estimated for carbonatitic liquids (Liu & Lange, 2003), while the uncertainty of the density would not produce a significant error in the calculated viscosity because of the large difference in densities between Pt sphere (ρ_s) and the carbonate-silicate melt density (ρ_l).

19.3. RESULTS

The run conditions and each calculated viscosity for synthetic carbonate-silicate melts are shown in Table 19.1. Figure 19.1 summarizes the P-T conditions of our experiments along with literature data where transitional melts were quenched. The short fall time of the Pt sphere results in high terminal velocity ranging between 0.749 and 6.628 mm/s. Figure 19.2 and Figure 19.3 show the fall of the Pt sphere through a series of radiographic images as a function of time, and the terminal velocity used to determine the viscosity through equation (19.1), respectively. The results of the falling distance as function of time and falling velocity for each run are available in the Supplementary Materials. The calculated viscosity of synthetic transitional melts varies from a minimum value of 0.0202(±0.0008) Pa·s at 2155 °C and 5.3 GPa and a maximum value of 0.0762(0.030) Pa·s at 1930 °C and 2.4 GPa. The viscosity data obtained for melts with ~18 wt% SiO_2 are shown in Figure 19.4, expressed in the logarithm form as function of pressure, along with previous studies on the viscosity of pure carbonate melts and carbonated silicate melts.

We carefully checked not only the falling of the sphere but also the lateral shift of the sphere during its fall, which might cause a decrease in the terminal velocity (Table 19.1). We observed that lateral shift ranges from 0.009 to 0.076 mm during the whole fall. These values are very low compared to the fall distance, where the terminal velocity is achieved (see Supplementary Materials). In contrast, we noted that lateral shift occurs mainly when the starting material begins melting as a consequence of the softening of the powder surrounding the Pt sphere at its initial position. Some experiments performed at P < 2 GPa showed the appearance of bubbles due to CO_2

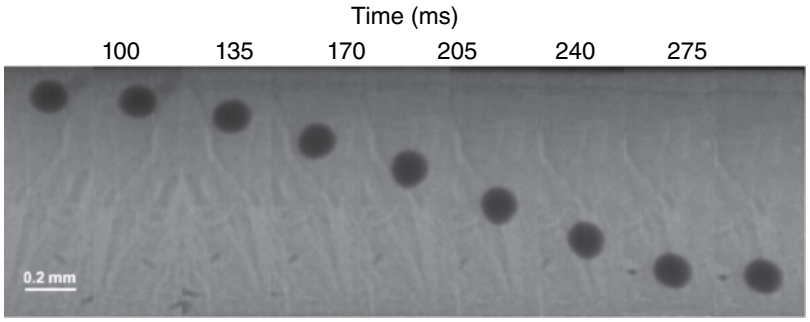

Figure 19.2 X-ray radiography images of the Pt sphere in carbonated silicate melt as function of time for experiment at 4.7 GPa and 2012 °C. See electronic version for color representation of the figures in this book.

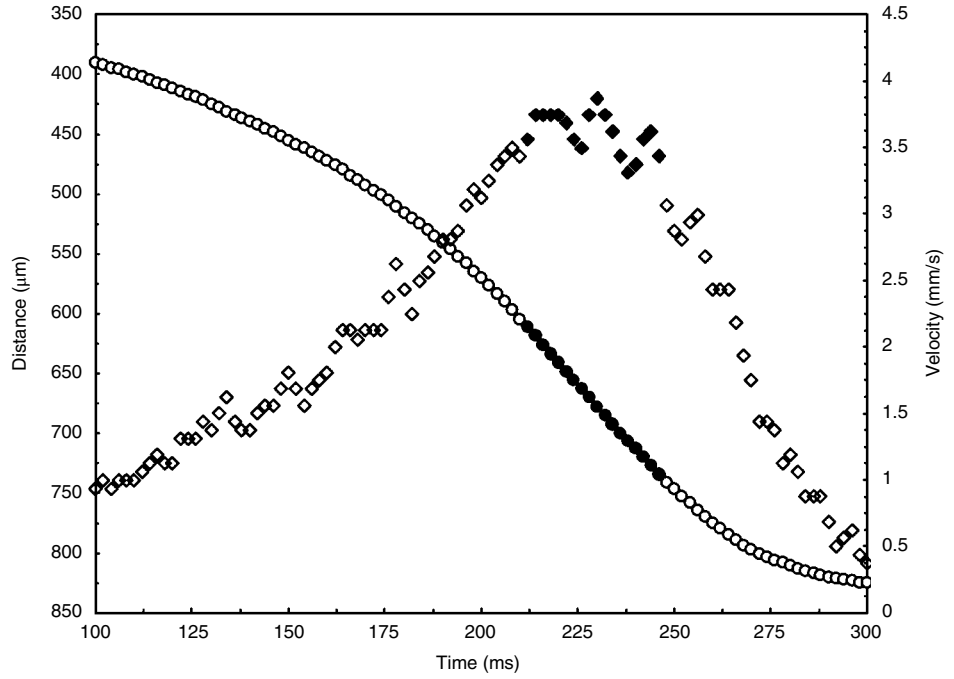

Figure 19.3 Results of the falling distance (circles) as function of time and the falling velocity (diamonds) as function of time for each frame (recording time is 500 fps) for the run at 4.7 GPa and 2012 °C. The terminal velocity reached by the sphere is indicated by filled symbols. See electronic version for color representation of the figures in this book.

exsolution that impeded the fall of the Pt sphere. These experiments are not presented here.

19.4. DISCUSSION

19.4.1. Effect of Pressure and Temperature on the Viscosity Data

Our data show viscosities between 0.0202 and 0.0762 Pa˙s, which are higher than those determined by Di Genova et al. (2016) and Stagno et al. (2018) for Na_2CO_3 melt, and Kono et al. (2014a) for calcitic and dolomitic melts by about an order of magnitude (Figure 19.4). The viscosity values for transitional melts appear comparable with data by Dobson et al. (1996) for molten $K_2Mg(CO_3)_2$ and $K_2Ca(CO_3)_2$ ranging from 0.006 to 0.036 Pa·s, taking into account the high uncertainty due to the lowest recording time (40 fps) employed by the authors with respect to more recent in-situ measurements. Figure 19.4 includes the viscosity of carbonated silicate melts performed on a $CaCO_3$-$CaSiO_3$ mixture with 22.6 and 31.4 wt% SiO_2, respectively (Kono et al., 2014a). These experiments yielded viscosities of 0.03 and 0.055 Pa˙s that are in agreement with our data. The viscosity calculated by molecular dynamics simulation by Ghosh and Karki (2017) covers a T range similar to our experimental conditions. Their calculations applied to enstatitic melts with 16 wt% of CO_2 gave a viscosity of 0.025 Pa˙s at 2200 K

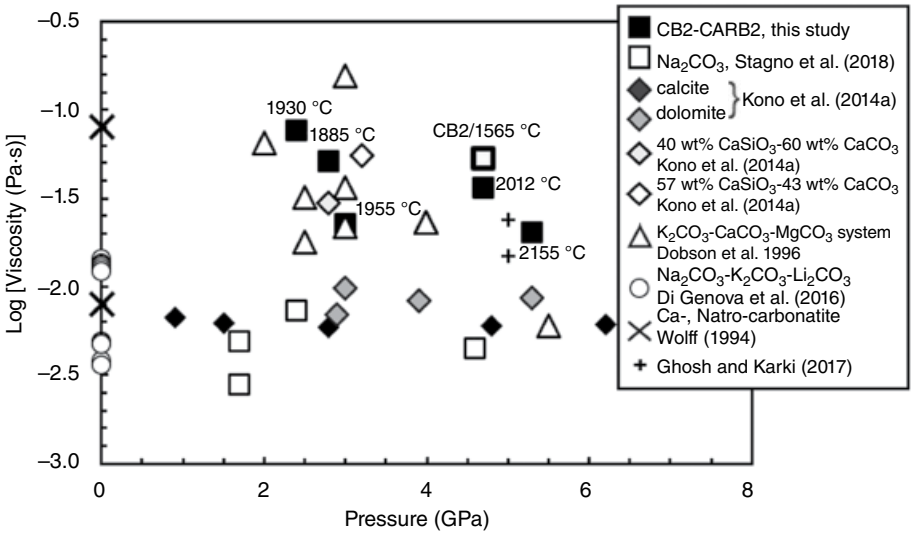

Figure 19.4 Experimentally determined viscosity data plotted as a function of pressure. Data from literature are reported for comparison. The uncertainty in our viscosity measurements is within the symbol size. See electronic version for color representation of the figures in this book.

and 5 GPa. Both experimental (Kono et al., 2014a) and theoretical (Ghosh & Karki, 2017) studies highlight the effect of temperature in lowering the viscosity of carbonated melts. This effect is also observable in Figure 19.4, where our data show a decrease in viscosity at increasing temperature of our experiments rather than a role of pressure. As also highlighted in Figure 19.1, our experiments were performed at much higher temperatures than the mantle adiabat. This is likely due to the higher liquid-glass transition temperature of the starting composition used in this study, linked with the chemical composition of the synthetic starting glassy material, although a possible kinetic effect on the melting process cannot be excluded.

To test the possible effect of the starting material, we performed an experiment (CB2_03_2015) using a mixture of oxides and carbonates. The viscosity determined at 4.7 GPa and only 1565 °C is 0.0529 Pa˙s (Table 19.1), which is higher than the viscosity determined for runs using CARB2. Although melting occurred at lower T, possibly due to the presence of absorbed moisture from the sample, we conclude that the fall of the sphere occurred at (near-)liquidus conditions. The viscosity determined at 4.7 GPa decreases from 0.0529 Pa˙s (run CB2_03_2015 at 1565 °C) to 0.0368 Pa˙s (run CARB2_3_2016 at 2012 °C) within about 400 °C. No obvious pressure effect can be claimed in our determined viscosities, similar to that reported by Stagno et al. (2018) for Na_2CO_3 melt and Kono et al. (2014a) for calcite and dolomite melts. Unfortunately, it remains difficult to collect isobaric data due to the pressure effect on the melting temperature of synthetic starting glasses.

19.4.2. Implications for the Transport of Oxidized Carbon in the Upper Mantle

The presence of small volumes of carbonate-silicate melts in the Earth's upper mantle has been the subject of several experimental studies aimed at understanding the origin of seismic (Hier-Majumder & Tauzin, 2017) and electrical (Gaillard et al., 2008; Yoshino et al., 2012) anomalies detected beneath mid-ocean ridges, as well as the immiscible behavior of CO_2-rich melts during upwelling and as their role in graphite/diamond precipitation or formation by redox melting during the Archaean (Aulbach & Stagno, 2016). Most of these processes imply interaction between migrating melts and host rock, causing CO_2-rich magmas to shift to transitional compositions. We calculated the mobility and migration rate of transitional melts using our determined viscosities. These were calculated using the equation

$$\phi w_0 = \frac{kg\Delta\rho}{\eta}, \tag{19.2}$$

with

$$k = \frac{a^2\phi^n}{C}, \tag{19.3}$$

where k is the permeability, a is the characteristic grain diameter, and ϕ is the melt fraction, while n (equal to 2) and C (equal to 1600) are numerical constants, g is the gravitational acceleration constant, and w_0 is the melt ascent velocity. As representative viscosity value, we considered 0.05 Pa·s, which leads to an average mobility, $\frac{\Delta\rho}{\eta}$, of transitional melts of ~25 g·cm^{-3}·Pa^{-1}·s^{-1}, assuming $\Delta\rho$

(density of the solid mantle-density of carbonate-silicate melt; Ghosh & Karki, 2017) equal to 1.2 $g \cdot cm^{-3}$ in the oceanic lithosphere. This value is between the mobility estimated for basalts of about 0.6 $g \cdot cm^{-3} \cdot Pa^{-1} \cdot s^{-1}$ (Sakamaki et al., 2013) and the high mobility of 148 $g \cdot cm^{-3} \cdot Pa^{-1} \cdot s^{-1}$ for Ca-carbonatitic melts calculated at upper mantle conditions (Kono et al., 2014a), even higher (300 $g \cdot cm^{-3} \cdot Pa^{-1} \cdot s^{-1}$) in the case of Na_2CO_3 liquid (Stagno et al., 2018). In turn, this implies a dramatic effect of the SiO_2 content of CO_2-rich magmas on their segregation and migration from the silicate mantle at solidus temperatures over time, enhancing, therefore, the possibility of melt-solid interaction and element diffusion. The calculation using equation (19.2) and equation (19.3) results in the melt migration velocity of ~1850 m/yr using a of 2 mm and melt fraction of 0.1% in volume, respectively (Keller et al., 2017). The migration velocity thus appears much higher than that proposed for dolomitic melts (80–115 m/yr; Kono et al., 2014a), implying that during the ascent of mantle carbonatitic magmas, as they evolve to more silica-rich compositions, the rheological properties might change dramatically, in turn promoting acceleration of these melts to shallower depth in contrast with a stagnant behavior of pure carbonatitic magmas. In contrast, long residence times are expected for carbonated magmas in the mantle.

19.5. CONCLUSIONS

We determined the viscosity of carbonated-silicate transitional melts with 18 wt% SiO_2 at pressures between 2.4 and 5.3 GPa (~70–160 km of depth) and temperatures between 1565 °C and 2155 °C. Results range between 0.02 and 0.08 Pa˙s with a variation mainly related to the temperature dependence. Our results agree with the sparse data from previous studies on $CaCO_3$-$CaSiO_3$ mixture (Kono et al., 2014a) and confirmed by dynamic simulation models on carbonated-$MgSiO_3$ melts (Ghosh et al., 2017). The higher viscosity compared to carbonatitic melt is therefore shown to correlate with the concentration of SiO_2. The relatively low ascent rate of transitional melts (~1850 m/yr) results in shorter residence time than carbonatitic melts within the upper mantle.

ACKNOWLEDGMENTS

V.S. gratefully acknowledges financial support from the Deep Carbon Observatory and Sapienza University of Rome through "Fondi di Ateneo 2016." This work was performed at HPCAT (Sector 16), Advanced Photon Source (APS), Argonne National Laboratory. HPCAT operation is supported by DOE-NNSA under Award No. DE-NA0001974, with partial instrumentation funding by the National Science Foundation. The Advanced Photon Source is a U.S. Department of Energy (DOE) Office of Science User Facility, operated for the DOE Office of Science by Argonne National Laboratory under Contract No. DE-AC02-06CH11357. The manuscript benefited from the thoughtful review of an anonymous referee and Stefano Poli. The authors also thank Claudia Romano and Brent T. Poe for the stimulating discussions that have supported some ideas in this paper.

SUPPLEMENTAL MATERIAL

CB2 at 4.7 GPa, 1565 °C

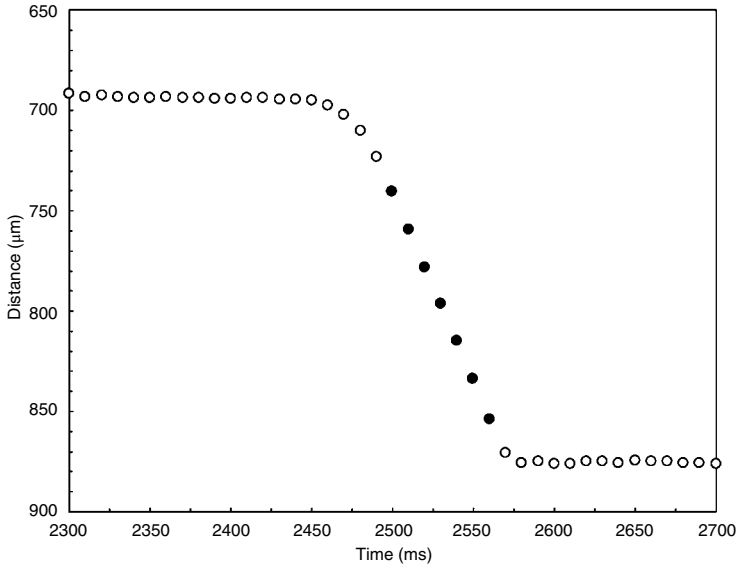

Figure S1 Results of the falling distance of the Pt sphere (117 μm) for the run at 4.7 GPa and 1565 °C as function of time.

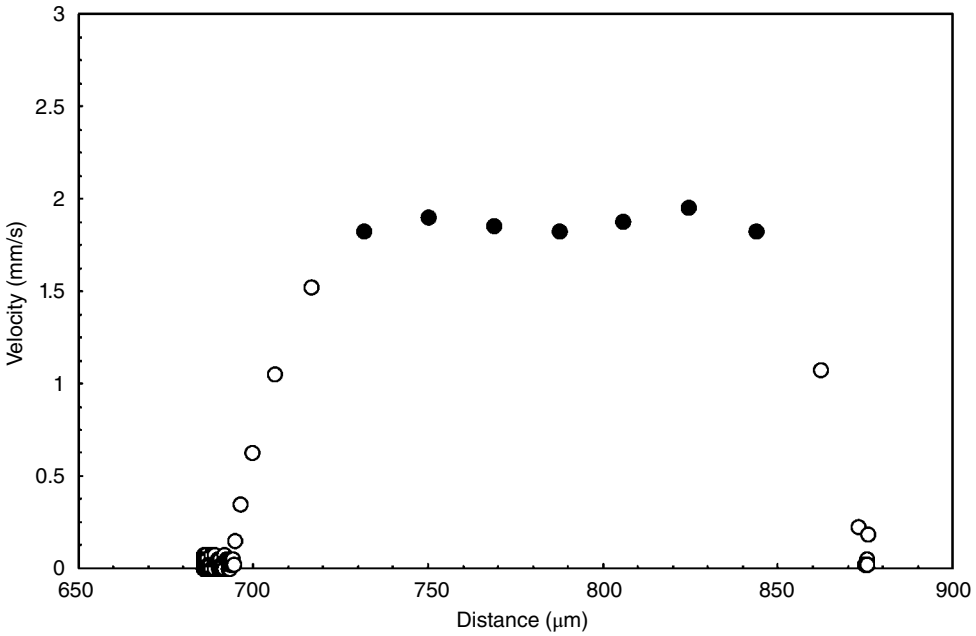

Figure S2 Results of the falling velocity of the Pt sphere for the run at 4.7 GPa and 1565 °C.

CARB2 at 2.8 GPa, 1885 °C

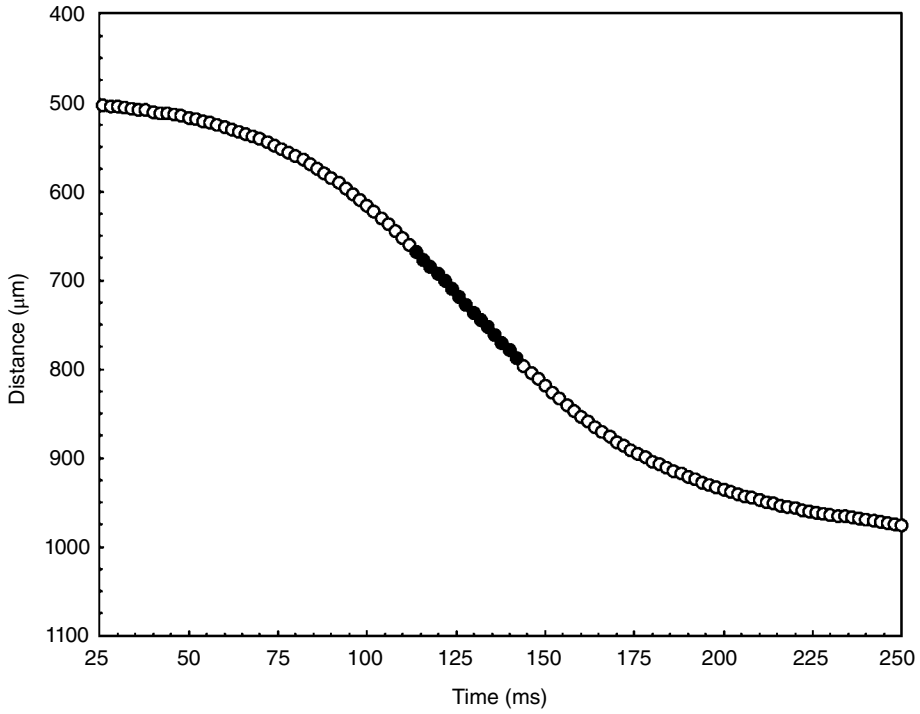

Figure S3 Results of the falling distance of the Pt sphere (191 μm) for the run at 2.8 GPa and 1885 °C as function of time.

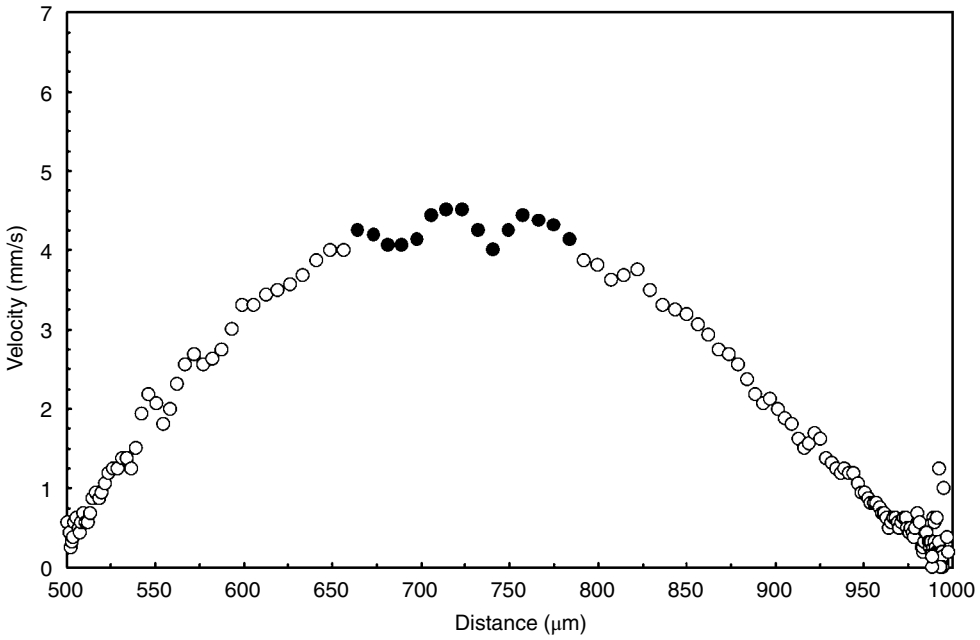

Figure S4 Results of the falling velocity of the Pt sphere for the run at 2.8 GPa and 1885 °C.

CARB2 at 4.7 GPa, 2012 °C

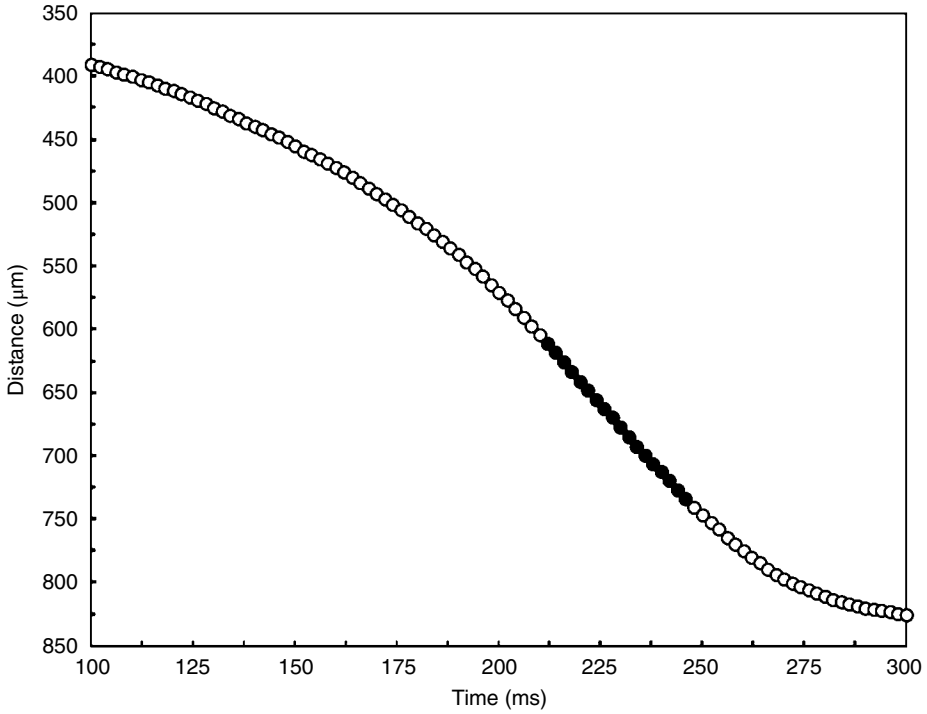

Figure S5 Results of the falling distance of the Pt sphere (140 μm) for the run at 4.7 GPa and 2012 °C as function of time.

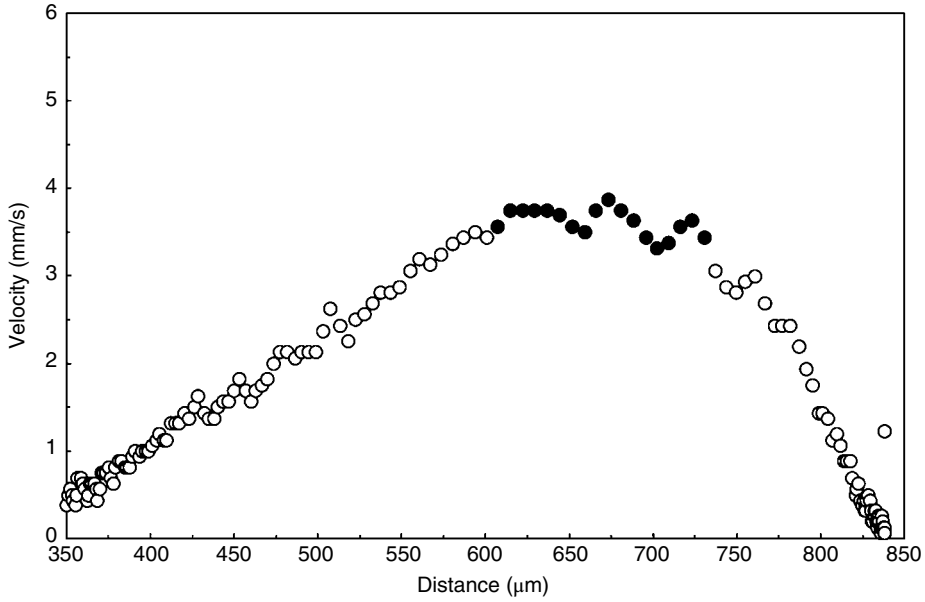

Figure S6 Results of the falling velocity of the Pt sphere for the run at 4.7 GPa and 2012 °C.

CARB2 at 5.3 GPa, 2155 °C

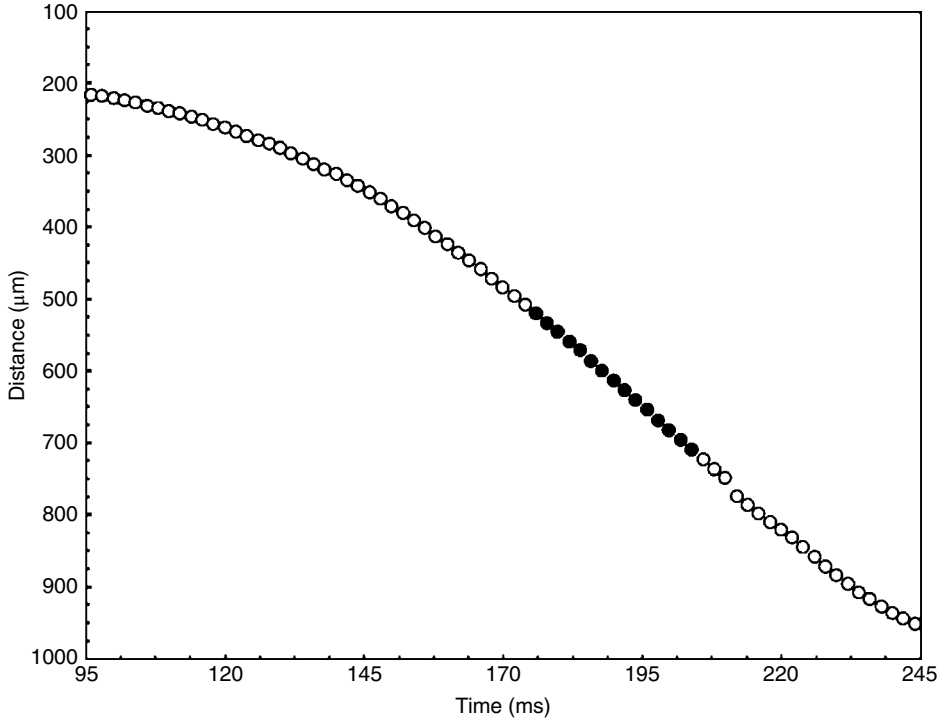

Figure S7 Results of the falling distance of the Pt sphere (140 μm) for the run at 5.3 GPa and 2155 °C as function of time.

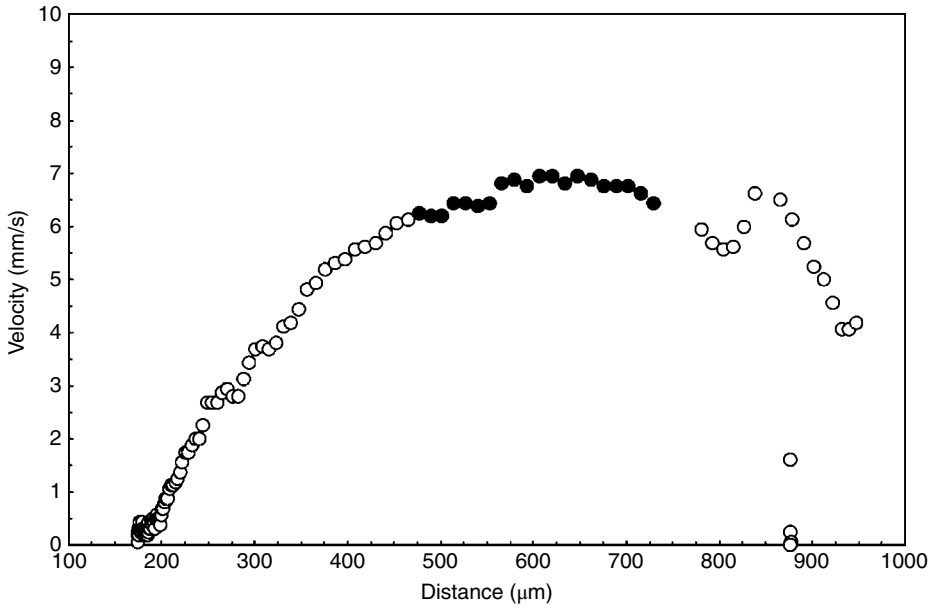

Figure S8 Results of the falling velocity of the Pt sphere for the run at 5.3GPa and 2155 °C.

CARB2 at 2.4 GPa, 1930 °C

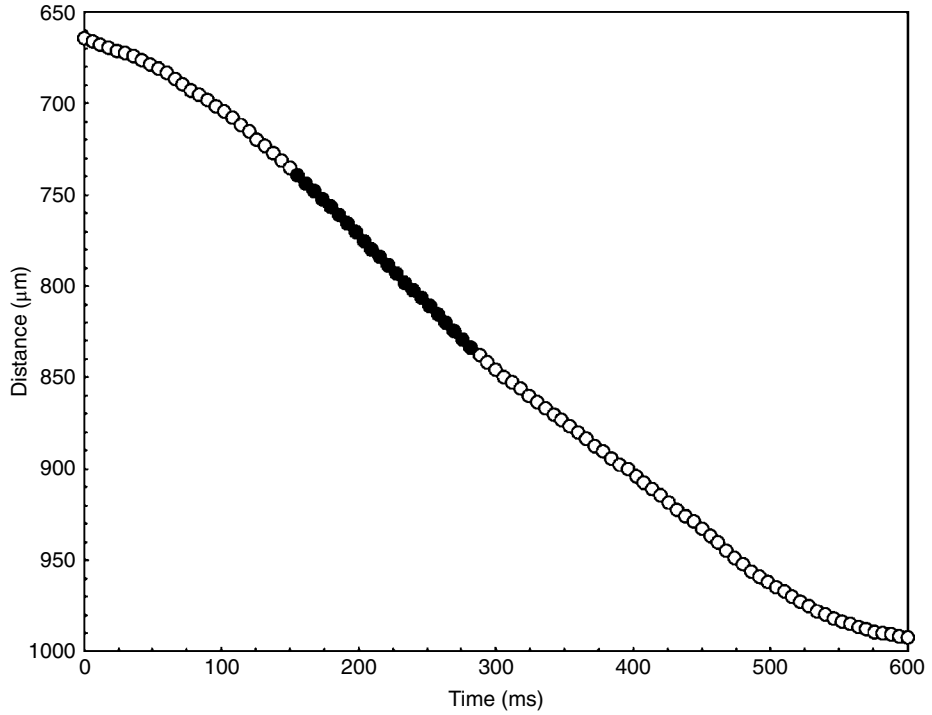

Figure S9 Results of the falling distance of the Pt sphere (86 μm) for the run at 2.4 GPa and 1930 °C as function of time. See electronic version for color representation of the figures in this book.

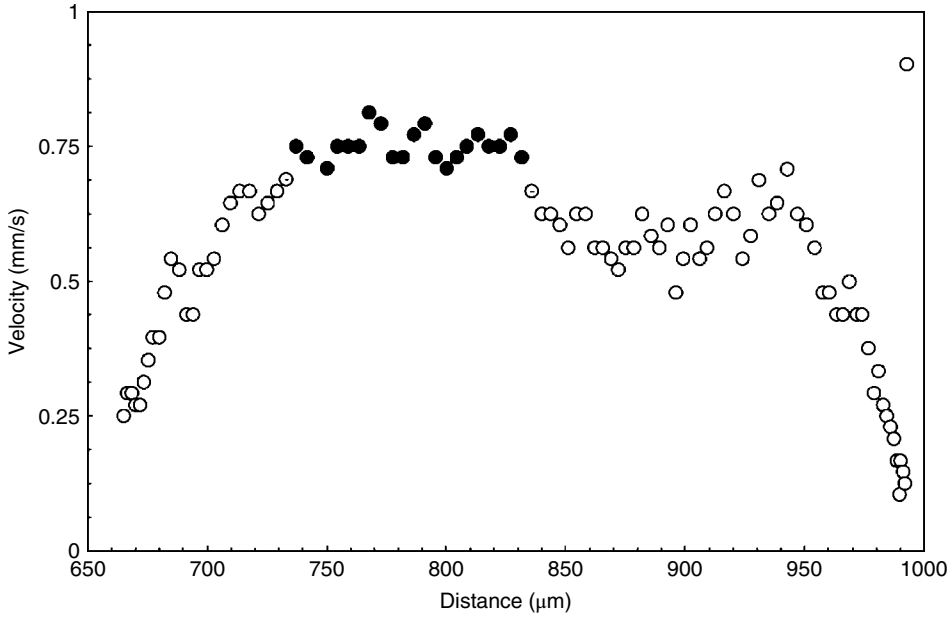

Figure S10 Results of the falling velocity of the Pt sphere for the run at 2.4 GPa and 1930 °C.

CARB2 at 3 GPa, 1955 °C

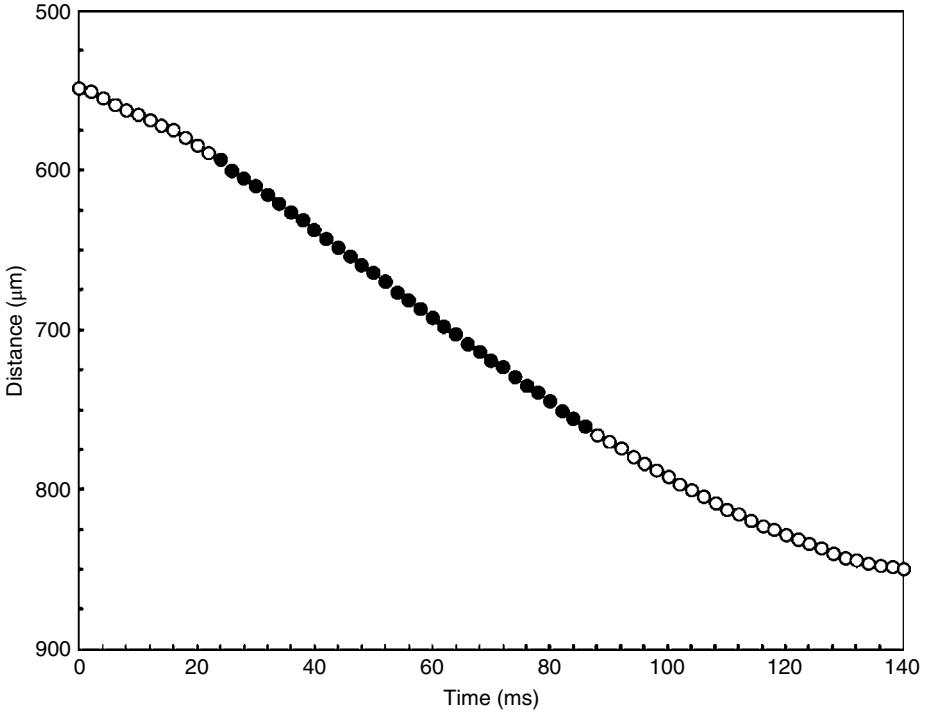

Figure S11 Results of the falling distance of the Pt sphere (89 μm) for the run at 3 GPa and 1955 °C as function of time.

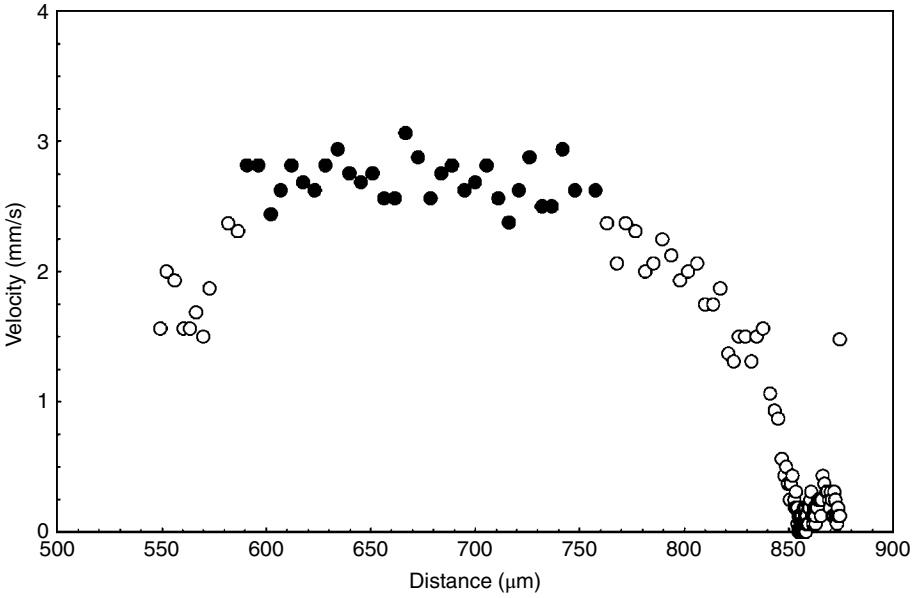

Figure S12 Results of the falling velocity of the Pt sphere for the run at 3 GPa and 1955 °C.

REFERENCES

Abramoff, M. D., Magalhaes, P. J., & Ram, S. J. (2004). Image processing with ImageJ. *Biophotonics International*, *11*, 7, 36–42.

Aulbach, S., & Stagno, V. (2016). Evidence for a reducing Archean ambient mantle and its effects on the carbon cycle. *Geology*, *44*, 751–754.

Brey, G. P., Bulatov, V. K., Girnis, A. V., & Lahaye, T. (2008). Experimental melting of carbonated peridotite at 6–10 GPa. *J. Petrol. 49*, 4, 797–821.

Brey, G. P., Bulatov, V. K., & Girnis, A. V. (2011). Melting of K-rich carbonated peridotite at 6–10 GPa and the stability of K-phases in the upper mantle. *Chem. Geol.*, *281*, 333–342.

Brooker, R. A., & Kjarsgaard, B. A. (2011). Silicate–carbonate liquid immiscibility and phase relations in the system SiO_2–Na_2O–Al_2O_3–CaO–CO_2 at 0. 1–2.5 GPa with applications to carbonatite genesis. *J. Petrol.*, *52*, 7&8, 1281–1305.

Dalton, J. A., & Presnall, D. C. (1998). Carbonatitic melts along the solidus of model lherzolite in the system CaO-MgO-Al_2O_3-SiO_2-CO_2 from 3 to 7 GPa. *Contrib Mineral Petrol*, *131*, 123–135.

Dasgupta, R., & Hirschmann, M. M. (2007). Effect of variable carbonate concentration on the solidus of mantle peridotite. *Am. Mineral.*, *93*, 370–379.

Dasgupta, R., Mallik, A., Tsuno, K., Withers, A. C., Hirth, G., & Hirschmann, M. M. (2013). Carbon-dioxide-rich silicate melt in the Earth's upper mantle. *Nature*, *493*, 211–216.

De Grouchy, C. J. L., Sanloup, C., Cochain, B., Drewitt, J. W. E., Kono, Y., & Crépisson, C. (2017). Lutetium incorporation in magmas at depth: Changes in melt local environment and the influence on partitioning behaviour. *Earth and Planetary Science Letters*, *464*, 155–165.

Di Genova, D., Cimarelli, C., Hess, K., & Dingwell, D. B. (2016). An advanced rotational rheometer system for extremely fluid liquids up to 1273 K and applications to alkali carbonate melts. *Am. Mineral.*, *101*, 953–959.

Dobson, D. P., Jones, A. P., Rabe, R., Sekine, T., Kurita, K., Taniguchi, T., et al. (1996). In-situ measurement of viscosity and density of carbonate melts at high pressure. *Earth Planet. Sci. Lett.*, *143*, 207–215.

Dorogokupets, P. I., & Dewaele, A. (2007). Equations of state of MgO, Au, Pt, NaCl-B1, and NaCl-B2: Internally consistent high-temperature pressure scales. *High Press. Res.*, *27*, 431–446.

Foley, S. F., Yaxley, G. M., Rosenthal, A., Buhre, S., Kiseeva, E. S., Rapp, R. P., & Jacob, D. E., (2009). The composition of near-solidus melts of peridotite in the presence of CO_2 and H_2O between 40 and 60 kbar. *Lithos*, *1125*, 274–283.

Gaillard, F., Malki, M., Iacono-Marziano, G., Pichavant, M., & Scaillet, B. (2008). Carbonatite melts and electrical conductivity in the asthenosphere. *Science*, *322*, 1363–1365.

Ghosh, S., Litasov, K., & Ohtani, E. (2014). Phase relations and melting of carbonated peridotite between 10 and 20 GPa: a proxy for alkali- and CO_2-rich silicate melts in the deep mantle. *Contrib Mineral Petrol*, *167*, 964.

Ghosh, D. B., Bajgain, S. K., Mookherjee, M., & Karki, B. B. (2017). Carbon-bearing silicate melt at deep mantle conditions. *Sci. Rep.*, *7*, 848.

Ghosh, D. B., & Karki, B. B. (2017). Transport properties of carbonated silicate melt at high pressure. *Sci. Adv.*, *3*, e1701840.

Gudfinnsson, G. H., & Presnall, D. C., (2005). Continuous gradations among primary kimberlitic, carbonatitic, melilitic, basaltic, picritic, and komatiitic melts in equilibrium with garnet lherzolite at 3–8 GPa, *J. Petrol.*, *46*, 1645–1659.

Hammouda, T. & Keshav, S. (2015). Melting in the mantle in the presence of carbon: Review of experiments and discussion on the origin of carbonatites. *Chem. Geol.*, *418*, 171–188.

Hier-Majumder, S., & Tauzin, B. (2017). Pervasive upper mantle melting beneath the western US. *Earth and Planetary Science Letters*, *463*, 25–35.

Hudspeth, J., Sanloup, C., & Kono, Y. (2018). Properties of molten $CaCO_3$ at high pressure. *Geochemical Perspectives Letters*, 17–21.

Keller, T., Katz, R. F., & Hirschmann, M. M. (2017). Volatiles beneath mid-ocean ridges: Deep melting, channelised transport, focusing, and metasomatism. *Earth Planet. Sci. Lett.*, *464*, 55–68.

Keshav, S., & Gudfinnsson, G. H. (2014). Melting phase equilibria of model carbonated peridotite from 8 to 12 GPa in the system CaO–MgO–Al_2O_3–SiO_2–CO_2 and kimberlitic liquids in the Earth's upper mantle. *Am. Mineral.*, *99*, 1119–1126.

Kiseeva, E. S., Yaxley, G. M., Hermann, J., Litasov, K. D., Rosenthal, A., & Kamenetsky, V. S. (2012). An experimental study of carbonated eclogite at 3˙5–5˙5 GPa: Implications for silicate and carbonate metasomatism in the cratonic mantle. *J. Petrol.*, *53*, 4, 727–759.

Kiseeva, E. S., Litasov, K. D., Yaxley, G. M., Ohtani, E., & Kamenetsky, V. S. (2013). Melting and phase relations of carbonated eclogite at 9–21GPa and the petrogenesis of alkali-rich melts in the deep mantle. *J. Petrol.*, *50*, 1555–1583.

Kono, Y., Irifune, T., Higo, Y., Inoue, T., & Barnhoorn, A. (2010). P-V-T relation of MgO derived by simultaneous elastic wave velocity and in-situ X-ray measurements: A new pressure scale for the mantle transition region. *Phys. Earth Planet. Inter.*, *183*, 196–211.

Kono, Y., Kenney-Benson, C., Hummer, D., Ohfuji, H., Park, C., Shen, G., et al. (2014a). Ultralow viscosity of carbonate melts at high pressures. *Nat. Commun.*, *5*, 5091.

Kono, Y., Park, C., Kenney-Benson, C., Shen, G., & Wang, Y. (2014b). Toward comprehensive studies of liquids at high pressures and high temperatures: Combined structure, elastic wave velocity, and viscosity measurements in the Paris–Edinburgh cell. *Phys. Earth Planet. Inter.*, *228*, 269–280.

Kono, Y. (2018). Viscosity measurement. In Y. Kono, & C. Sanloup (Eds.), *Magmas under pressure: Advances in high-pressure experiments on structure and properties of melts*. (pp. 261–280). Elsevier.

Litasov, K. D., & Ohtani, E. (2009a). Phase relations in the peridotite-carbonate-chloride system at 7. 0–16. 5 GPa and the role of chlorides in the origin of kimberlite and diamond. *Chemical Geology*, *262*, 29–41.

Litasov, K. D., & Ohtani, E. (2009b). Solidus and phase relations of carbonated peridotite in the system CaO-Al_2O_3-MgO-SiO_2-Na_2O-CO_2 to the lower mantle depths: *Physics of the Earth and Planetary Interiors*, *177*, 46–58.

Litasov, K. D., & Ohtani, E. (2010). The solidus of carbonated eclogite in the system CaO–Al_2O_3–MgO–SiO_2–Na_2O–CO_2 to 32 GPa and carbonatite liquid in the deep mantle. *Earth Planet. Sci. Lett.*, *295*, 115–126.

Liu, Q., & Lange, R. A. (2003). New density measurements on carbonate liquids and the partial molar volume of the $CaCO_3$ component. *Contrib. Mineral. Petrol.*, *146*, 370–381.

Martin, L.H.J., Schmidt, M. W., Mattsson, H. B., & Guenther, D. (2013). Element partitioning between immiscible carbonatite and silicate melts for dry and H_2O-bearing systems at 1–3 GPa, *Journal of Petrology*, *54*, 11, 2301–2338.

Masotta, M., Freda, C., Paul, T. A., Moore, G. M., Gaeta, M., Scarlato, P., & Troll, V. (2012). Low pressure experiments in piston cylinder apparatus: Calibration of newly designed 25 mm furnace assemblies to P = 150 MPa. *Chem. Geol., 312–313*, 74–79.

Moore, K. R., & Wood, B. J. (1998). The transition from carbonate to silicate melts in the CaO–MgO–SiO_2–CO_2 system. *J. Petrol.*, *39*, 1943–1951.

Moussallam, Y., Morizet, Y., Massuyeau, M., Laumonier, M., & Gaillard, F. (2015). CO_2 solubility in kimberlite melts. *Chem. Geol.*, *418*, 198–205.

Rohrbach, A., & Schmidt, M. W. (2011). Redox freezing and melting in the Earth's deep mantle resulting from carbon–iron redox coupling. *Nature*, *472*, 209–212.

Sakamaki, T., Suzuki A., Terasaki H., Urakawa S., Katayama Y., Funakoshi K., et al. (2013). Ponded melt at the boundary between the lithosphere and asthenosphere, *Nat. Geosci.*, *6*, 1041–1044.

Stagno, V., & Frost, D. J. (2010). Carbon speciation in the asthenosphere: Experimental measurements of the redox conditions at which carbonate-bearing melts coexist with graphite or diamond in peridotite assemblages. *Earth. Planet. Sci. Lett.*, *30*, 72–84.

Stagno, V., Ojwang, D. O., McCammon, C. A., & Frost, D. J. (2013). The oxidation state of the mantle and the extraction of carbon from Earth's interior. *Nature*, *11679*, 493.

Stagno, V., Stopponi, V., Kono, Y., Manning, C. E., & Irifune, T. (2018). Experimental determination of the viscosity of Na_2CO_3 melt between 1. 7 and 4. 6 GPa at 1200–1700 °C: Implications for the rheology of carbonatite magmas in the Earth's upper mantle. *Chem. Geol.*, *501*, 19–25.

Stixrude, L., & Lithgow-Bertelloni, C. (2007). Influence of phase transformations on lateral heterogeneity and dynamics in Earth's mantle. *Earth Planet. Sci. Lett.*, *263*, 45–55.

Terasaki, H., Kato, T., Urakawa, S., Funakoshi, K. I., Suzuki, A., Okada, T., & Kasai, S. (2001). The effect of temperature, pressure, and sulfur content on viscocity of the Fe-FeS melt. *Earth and Planetary Science Letters*, *190*(1–2), 93–101.

Wolff, J. A. (1994). Physical properties of carbonatite magmas inferred from molten salt data, and application to extraction patterns from carbonatite–silicate magma chambers. *Geol Mag*, *131*, 145–153.

Yoshino, T., McIsaac, E., Laumonier, M., & Katsura, T. (2012). Electrical conductivity of partial molten carbonate peridotite, *Physics of the Earth and Planetary Interiors*, *194–195*, 1–9.